

Model Predictive Control for Power and Thermal Management of an Integrated Solid Oxide Fuel Cell and Turbocharger System

So-Ryeok Oh, Jing Sun, *Fellow, IEEE*, Herbert Dobbs, and Joel King

Abstract—This paper identifies and addresses the control challenges associated with simultaneous power and thermal management of a 5-kW-class solid oxide fuel cell and gas turbine combined cycle system. A model predictive controller (MPC) is developed to achieve improved system performance subject to input and state constraints. The subsystem dynamic couplings and control authority limitations under thermal constraints are investigated by both static and dynamic analysis. Through judicious allocation of penalty parameters in the cost function associated with the fuel cell current, anode fuel flow rate, and generator load, several different MPC implementations are derived to explore different control design degree of freedom and their performance is evaluated. Simulation results show the efficacy of the MPC design by demonstrating the fast load transition while maintaining the stack temperature within the allowable operation limits.

Index Terms—Model predictive control, power and thermal management, SOFC/GT hybrid system.

NOMENCLATURE

| | |
|----------------------|--|
| $c_{(\cdot)}$ | Heat capacity (J/kg·K). |
| F | Faraday's Constant (C/mol). |
| h_i | Enthalpy of species i (J/kg). |
| J | Shaft inertia (kgm ²). |
| I | Current density (A/m ²). |
| m | Mass (kg). |
| W | Flow rate (kg/s). |
| N | Shaft rotational speed (rpm). |
| n_i | Molar rate of species i (mol/s). |
| $p_{(\cdot)}$ | Pressure of (\cdot) (Pa). |
| $P_{\text{NET/GEN}}$ | Net/generator power (W). |
| \bar{R} | Universal gas constant (J/K·mole). |
| R_{ohm} | Cell resistance ($\Omega \cdot \text{m}^2$). |
| T | Temperature (K). |
| U | Voltage (V). |

Manuscript received August 27, 2012; revised February 8, 2013 and May 20, 2013; accepted June 8, 2013. Manuscript received in final form June 27, 2013. Date of publication August 29, 2013; date of current version April 17, 2014. This work was supported in part by the U.S. Army TARDEC through Automotive Research Center and U.S. Navy through Naval Engineering Education Center, both led by the University of Michigan. Recommended by Associate Editor F. A. Cuzzola.

S.-R. Oh and J. Sun are with the Department of Naval Architecture and Marine Engineering, University of Michigan, Ann Arbor, MI 48109 USA (e-mail: srohum@umich.edu; jingsun@umich.edu).

H. Dobbs and J. King are with the U.S. Army TARDEC, Warren, MI 48397 USA (e-mail: herbert.dobbs@us.army.mil; joel.d.king@us.army.mil).

Color versions of one or more of the figures in this paper are available online at <http://ieeexplore.ieee.org>.

Digital Object Identifier 10.1109/TCST.2013.2271902

| | |
|--------|---------------------------------|
| V | Volume (m ³). |
| η | Efficiency. |
| x_i | Molar fraction of species i . |

I. INTRODUCTION

IMPROVING energy system efficiency of mobile and stationary power generation has been an imperative strategic direction to achieve energy security and environmental sustainability, especially for those power plants based on fossil fuels. Given the global focus on energy and environmental issues, power generation technologies that have advantages on energy efficiency and environmental impact are attracting more attentions. Those systems are often of hybrid nature in which they integrate multiple power sources to exploit their complementary features for improved energy efficiency and reduced environmental impact. Solid oxide fuel cells (SOFCs), which operate at elevated temperatures ($\sim 1000^\circ\text{K}$), are particularly well suited to combine with a gas turbine (GT) to form a bottoming cycle in a hybrid SOFC/GT configuration. The efficiency of such an integrated system can potentially exceed 60% and even approach 70% for future optimized designs [1]–[4]. In addition to its advantages in energy efficiency and environmental friendliness, its internal reforming feature also makes the SOFC/GT hybrid technology flexible in fueling and capable of operating with natural gas, coal, or biomass fuel.

Interest in the SOFC/GT hybrid cycle has been increased in recent years. The integration of SOFC/GT was first considered for the stationary power plant applications [5]. With the advent of small GTs (rating less than multihundred kilowatt), and with the maturing of the modular fuel cells, the high-performance hybrid cycle systems have started showing their promise for low power applications on mobile platforms, such as auxiliary aerospace power unit [6], unmanned aerial vehicles [7], [8] over high altitude and long endurance missions, marine power generation [9], [10]. Performance analysis and component sizing have also been addressed in recent literature, such as in [11] and [12]. In particular, for turbines of large sizes, there is considerable design freedom to vary the pressure ratio and air flow rate while maintaining a high level of overall efficiency for high power output. In contrast, micro GTs with a single-stage compressor have a limited pressure ratio and may not have substantial advantages in terms of overall efficiency over a stand-alone SOFC at that scale.

Although the design and optimization of SOFC/GT system have been pursued by the research and engineering

communities for many years, the control and system integration solutions, especially those aimed at explicitly addressing the operational constraints, have not been fully explored. In [6], the power, fuel utilization (FU), and cell temperature in an SOFC/GT system have been controlled by manipulating the current, fuel, and air feed flow rates, using a proportional–integral–differential (PID) control. In the referred work, several multiloop controllers have been put in place to keep the FU and temperature within the safe operating limits. Even though there are strong interactions among different loops in the system, the decentralized multiloop control design could be made stable because of the timescale separation of those loops. In [14], I/O pairing was established to gain the full benefit of a decentralized controller, and a power operation line was selected from the performance map to keep the fuel cell temperature fairly constant under part-load conditions. [15] proposes a control strategy for the bottoming of SOFC/GT hybrid system based on a linearized model.

It is noted that the SOFC/GT hybrid system relies on close coupling of subsystems to achieve its high efficiency. It exhibits highly nonlinear characteristics and subjects to physical constraints that has to be strictly enforced to assure safe and efficient operation. The authors of [16] developed a dynamic model of an SOFC/GT system and evaluated the matching between the model and a linearized version of the same model. They noted that the linear and nonlinear model responses match only with a small range of variations in the inputs, and concluded that the nonlinearities cannot be ignored in the performance evaluation. The review of the literature indicates that a nonlinear model predictive control (MPC) can be an attractive option for the SOFC/GT system because of its capabilities in handling constraints and nonlinearities, and its flexibility in accommodating different design considerations and performance indices. To the best knowledge of the authors, the control development of SOFC/GT reported in literature has not explored the MPC to explicitly handle physical and operation constraints, except that presented in [25].

This paper aims at developing a model-based control scheme to address the load following and temperature control problems of the constrained SOFC/GT hybrid system. In particular, the previous control study of the one-step MPC reported in [25] is extended to the multistep MPC to address the nontrivial challenges because of the operational constraints and close coupling between power and temperature control. On the basis of a high fidelity model developed in [23], in-depth analysis is carried out to understand the control authority of the inputs and operational constraints for transient load control and thermal management. The analysis reveals the key challenges that necessitate more sophisticated and systematic design approach, and also points to the direction of MPC development. To facilitate the design of MPC, a reduced-order nonlinear model amenable for online optimization is derived, with special attention paid to computational efficiency. The model is validated against a high-fidelity model presented in [23].

The remainder of this paper is organized as follows. Operating principles for the SOFC/GT hybrid system are briefly presented Section II, followed by the analysis of the operating

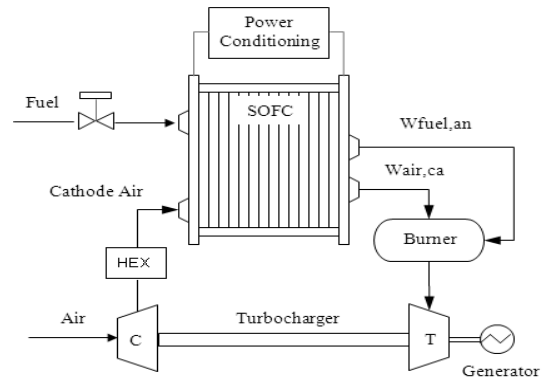


Fig. 1. SOFC/GT hybrid schematic.

constraints that highlight the challenges of simultaneous power tracking and thermal management. Section III presents a low-order nonlinear lumped parameter model for the hybrid power plant, with validation results against a high fidelity model. In Section IV, an MPC for the power and SOFC temperature. Management is designed, followed by the simulation results and discussions. Finally, concluding remarks are stated in Section V.

II. SOFC/GT OPERATING PRINCIPLES AND CONTROL PROBLEM FORMULATION

The hybrid SOFC/GT system analyzed in this paper is designed as an auxiliary power unit (APU) targeting military and commercial applications. For example, this unit can be used in a commercial vehicle to reduce the amount of time the main engine spends idling, thereby improve efficiency and reduce emissions. For military trucks, the proposed APU can provide sufficient power to support silent watch and other missions without involving the main engine. The system has a rated power 5 kW.¹ The key system components include an SOFC stack, a compressor (C), a catalytic burner (CB), a heat exchanger, a turbine (T) which drives a generator (GEN) and powers the compressor, as shown in Fig. 1. Other components, such as the reformer, are not included in this paper to focus on the coupling dynamics between the SOFC and GT.

A. Operating Principles

There are two power generation units in the SOFC/GT system: the SOFC and the generator. Therefore, the reliable operation and overall system efficiency will be a result of judicious coordination of the control inputs to the two power plants. Air is supplied to the cathode side of SOFC by the compressor, while prereformed fuel is fed to the anode side. The exhaust from the SOFC outlet passes through the CB where the unused fuel is burned to increase the temperature and pressure of the flow. The high temperature and high

¹Although the typical power rating for SOFC/GT systems is much higher than 5 kW, the choice of the power rating for the system considered in this paper is dictated by the available project resources. However, the control problems and operating constraints discussed in this paper are generic for SOFC/GT hybrid systems. The rated power can be scaled by simply changing the number of the individual fuel cells.

pressure flow from the CB then powers the turbine, thereby providing a mechanism to recuperate the exhaust energy. Fig. 1 shows that the turbine drives both the compressor and the generator through a mechanical shaft. The former delivers the air and the latter provides additional electrical power to the system.

B. Power and Temperature Control Under Operating Constraints

The primary control objective of the integrated SOFC/GT, targeted for mobile applications, is to meet the varying power demand. In addition, keeping the cell temperature within certain bounds is an essential operational requirement. High temperature can affect the fuel cell catalyst, and temperature fluctuations during the transient can cause thermal fatigue, thereby affecting the long-term electrochemical performance. Hence, the mean cell temperature should be maintained as constant as possible throughout the part-load operation.

Besides the power and temperature control objectives, there are many other physical constraints that dictate the dynamic operation of the SOFC/GT systems. Those constraints include, but are not limited to:

- 1) *SOFC FU Limitation*: Although very low FU of the SOFC would lead to low system efficiency and high burner temperature, very high FU could cause local fuel starvation that can lead to irreversible damage of the fuel cells. The FU should be controlled around its optimal points (85% in this case) and excursions in FU should be minimized;
- 2) *SOFC Current and Power Rate Limit*: Large and sudden changes in current and power can cause fuel and current out of synchronization, thereby leading large local mechanical and thermal stress;
- 3) turbine and compressor stall and surge limits;
- 4) catalytic burner temperature and turbine inlet temperature limits.

In addition to power tracking, thermal management, and constraint enforcement, the control system also has to manipulate the inputs to achieve optimal energy efficiency.

C. Static Optimization and Feedforward Control

For steady-state operation, the main objective of the SOFC/GT system is to achieve maximum fuel efficiency. Model-based optimization can be performed to determine the optimal combination of inputs, namely the fueling rate, stack current, and generator load, to achieve the highest system efficiency while satisfying relevant constraints [19]. For example, for a given fuel flow, different combinations of current drawn from the SOFC and load applied to the generator will yield different net power. To determine the maximum steady-state net power output for a given fuel flow W_{Fuel} , the following optimization problem, with proper constraints can be solved

$$\max_{I_{\text{com}}, P_{\text{GEN}}} \eta_{\text{SOFC/GT}} \quad (1)$$

By repeating the optimization problem for different fuel flows, the optimal steady-state operation points are obtained

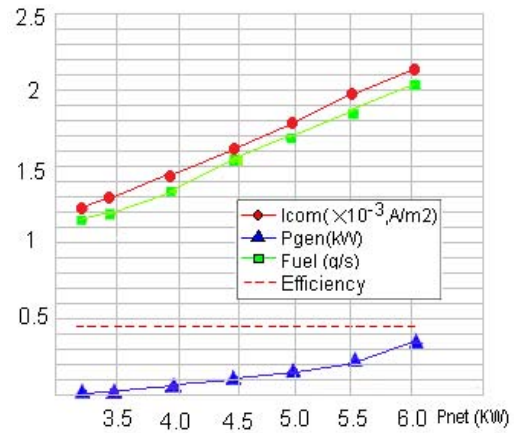


Fig. 2. Steady-state optimal set points for current density, fuel, generator load, and efficiency as a function of load.

as shown in Fig. 2, which depicts the current density from the SOFC unit, the required fuel flow and the power delivered by the generator as functions of the desired net power generated by the integrated system. The power of the hybrid SOFC–GT model is in the range 0–6 kW. As shown in Fig. 2, no power is produced from a micro GT in the range 0–3 kW. In addition, the overall efficiency of the SOFC/GT system is 45% regardless of the load.

The results can be easily implemented with a look-up table and used as static feedforward maps to schedule the actuators and power split to achieve the maximum steady-state efficiency for different power demands. Moreover, rate limiters can be imposed for the feedforward control to satisfy the current and power rate limit constraints for transient operation.

D. Dynamic Analysis and Feedback Control Challenges

Although the feedforward maps shown in Fig. 2 provides an easy way to schedule the inputs according to the power demand, managing transients with both the power tracking and thermal management constraints are a difficult task. In this section, we analyze the dynamic characteristics exhibited by SOFC/GT system in the following two scenarios to highlight the special control challenges.

Scenario 1: Power transition with temperature and current rate limit constraints. Consider the transition from part load [point A at the lower left corner of Fig. 3(a)] to full load [point B at the upper right corner of Fig. 3(a)] operation or vice versa. Without sophisticated feedback control, we have two options, namely: 1) stepping up (or down) immediately from A to B by changing the input set points according to Table I or 2) moving slowly from A to B by following the line shown in Fig. 3(a) and with the help of the feedforward maps shown in Fig. 2. Conventional wisdom, reinforced by the current and power rate limit constraints, would suggest strategy (2). However, note that the temperature along the line AB in Fig. 3(a) will go through the transition shown in Fig. 3(b), thereby exacerbating the temperature management problem. To avoid temperature overshoot during the transient, the fast transition (step up from A to B) should be favored. Fig. 3(c) and (d) shows the dynamic simulation results with one fast and one slow power transition.

TABLE I

LOAD CHANGE SCENARIO FROM LOW LOAD (A) TO HIGH LOAD (B)

| | $W_{Fuel}(kg/s)$ | $I_{COM}(A/m^2)$ | $P_{GEN}(W)$ | $P_{NET}(W)$ |
|---|------------------|------------------|--------------|--------------|
| A | $1.85e^{-3}$ | 1910 | 175 | 5300 |
| B | $2.08e^{-3}$ | 2100 | 350 | 5900 |

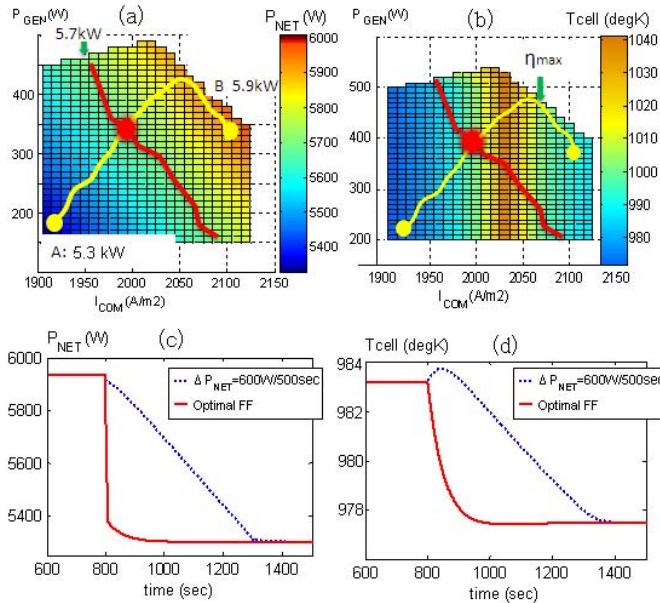


Fig. 3. (a) and (b) Power and temperature 2-D plots. Constant power line (red) and most efficiency line (yellow) from low power (A) to high power (B). (c) Simulation with fast and slow power transition and (d) the corresponding temperature responses.

We can see that the temperature response with fast transition gives better performance in terms of not causing temperature overshoot. However, fast power transition may excite other transient issues and is often limited by a current or power rate limiter.

Scenario 2: Maintaining constant power while regulating the SOFC temperature. For controlling the temperature of SOFC while keeping the power constant, there are two fast actuation mechanisms: the fuel cell current and the generator load. However, along the constant power line (shown in Fig. 3(a) as the red line), the temperature variation is nonmonotonic as the current (or the generator load) increases (or decreases), as shown in Fig. 4.

Because air is used as a coolant for SOFC and increase or decrease in air flow is controlled by the generator load P_{gen} , conventional wisdom suggests that an increase in P_{GEN} will reduce the shaft speed and therefore lead to an increase in temperature because of reduced air flow. However, an increase in P_{GEN} at the same time reduces the power generation in SOFC as power is maintained constant, which in turn reduces the electrochemical activities and heat generation. The coexistence of these two opposing mechanisms causes the nonmonotonic sensitivity in cell temperature and dictates that simple PID type controllers will not be effective in regulating the temperature over a wide range of operating conditions.

The two aforementioned examples highlight the difficulties in dynamic control of the SOFC/GT systems for simultaneous

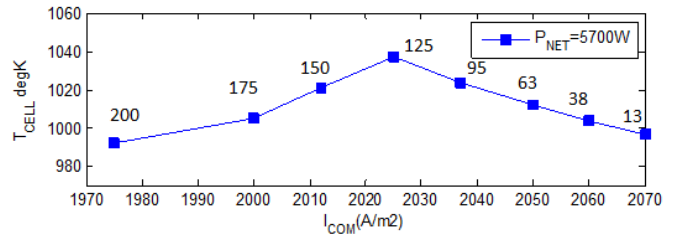


Fig. 4. Nonmonotonic temperature variation along the constant power line.

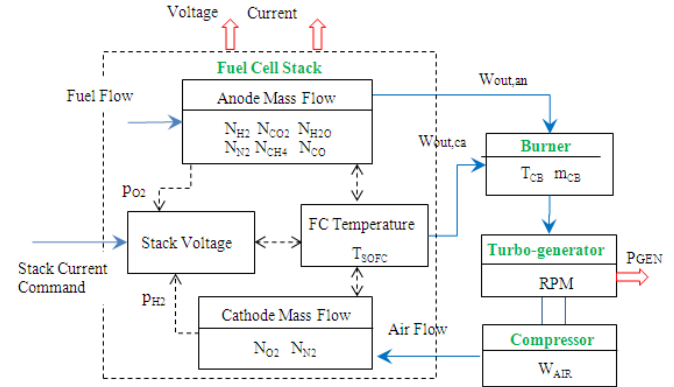


Fig. 5. SOFC system model block diagram.

power tracking and temperature regulation. Given the non-linear and highly coupled dynamics of the system, and the importance of enforcing operating constraints, MPC emerges as a natural candidate of the control approach. The control-oriented model is presented in Section III to facilitate the design and implementation of MPC.

III. REDUCED-ORDER MODEL FOR MPC DESIGN

Several dynamic models can be found in literature for SOFC/GT systems, including those developed by [19] and [23], as well as those by other groups [6], [16], [20].

In [23], the SOFC stack volume has been divided into 4(axial) \times 5(radial) lumped control volumes to capture the transient gas and thermal behavior, as well as their spatial distributions. The system model block diagram, showing the subsystem blocks and their interactions along with inputs and outputs, is shown in Fig. 5. The overall system model comprises 47 nonlinear coupled ordinary differential equations as well as many nonlinear functions and look-up tables (such as those for the compressor and turbine maps) and therefore is not amenable to real-time optimization and MPC implementation. In this section, we focus on developing a low-order lumped parameter nonlinear model that can be used for MPC design. To this end, the pressure and temperature are assumed to be uniform within the entire SOFC stack. The proposed model has five dynamic states, namely the cell temperature and pressure, shaft speed, CB temperature, and mass.

A. Model Development

The mathematical description of main component models, such as these for SOFC, GT, and compressor, and catalytic

burner, is provided in detail as follows. First principles such as mass and energy conservation are used in the model development. Important variables such as temperature, pressure, mass flow rate, and species fraction are also considered in each component model.

An SOFC model is developed using mass balance and energy balance. The following main assumptions are made in developing a simplified nonlinear model.

- 1) All the physical variables including the gas temperatures and pressures are assumed to be uniform along the flow axis in the SOFC stack, resulting in a lumped parameter fuel cell model.
- 2) All gases are assumed to be ideal.
- 3) All cells in the stack are assumed to operate identically.
- 4) Compressor flow, pressure, and power characteristics are modeled using performance maps [19].
- 5) N_2 , H_2 , CH_4 , H_2O , CO , CO_2 are assumed to be the species in the flow through the fuel channel and N_2 , O_2 through the air channel.

The output stack voltage U is defined as a function of the stack current, reactant partial pressures, and fuel cell temperature

$$U = U_{OCV} - (V_{act} + V_{con} + V_{ohm}). \quad (2)$$

Equation (2) is the standard polarization function, U_{OCV} is the open circuit voltage determined by the Nernst equation [17]. The last three terms represent various potential losses. The activation loss, V_{act} , as a result of energy barriers is to be overcome for the electrochemical reaction to occur, and can be characterized by the Butler–Volmer equation. The concentration loss, V_{con} , reflects the overpotential because of the species diffusion between the reaction site and the bulk flow in gas channels, and V_{ohm} is the ohmic loss because of the electrical and ionic resistance along the path of the current in the fuel cell. The ohmic, activation, and concentration losses are calculated according to the procedure discussed in [17] and [18].

The stack temperature and pressure are determined from the energy conservation equations and the ideal gas law, respectively [28]

$$\frac{dT_S}{dt} = \frac{1}{mc_v} \left[W_S^i c_v (T_S^i - T_S) - R(T_i W_S^i - T_S W_S^o) + Q \right] \quad (3)$$

$$\frac{dp_S}{dt} = \frac{R}{V_S} \left[(W_S^i - W_S^o) T_S + m \frac{dT_S}{dt} \right] \quad (4)$$

where the subscript “S” stands for SOFC, the superscripts “i” and “o” stands for inlet and outlet. Q , the total heat released because of electrochemical reactions, is equated to

$$Q = \frac{I}{2F} [h_{H_2} + 0.5h_{O_2} - h_{H_2O}] - IU. \quad (5)$$

With the gas reaction process within the fuel cell shown in [23], the species outlet flow rates $n_{(\cdot)}^o$ are related to the inlet fuel flow n_F^i and the stack current I through the following

equation:

$$\begin{bmatrix} n_{H_2}^o \\ n_{H_2O}^o \\ n_{CO}^o \\ n_{CO_2}^o \\ n_{CH_4}^o \end{bmatrix} = \begin{bmatrix} n_{H_2}^i \\ n_{H_2O}^i \\ n_{CO}^i \\ n_{CO_2}^i \\ 0 \end{bmatrix} + \begin{bmatrix} -\frac{1}{2F} & 3x_{CH_4}^i & -1 \\ \frac{1}{2F} & -x_{CH_4}^i & 1 \\ 0 & x_{CH_4}^i & 1 \\ 0 & 0 & -1 \\ 0 & 0 & 0 \end{bmatrix} \begin{bmatrix} I \\ n_F^i \\ \Delta n_{CO} \end{bmatrix} \quad (6)$$

where Δn_{CO} is the difference of CO in the inlet and outlet streams and it is computed using the water gas shift reaction given by [17]

$$\frac{n_{CO_2}^o \cdot n_{H_2}^o}{n_{CO}^o \cdot n_{H_2O}^o} = K_{eq,WGS} \quad (7)$$

with $K_{eq,WGS} = \exp(4276/T_S - 3.961)$.

Defining $n_F^o = \sum n_k^o$ and $n_F^i = \sum n_k^i$, where $k = \{H_2, \dots, N_{CH_4}\}$, we can show from (6) that

$$n_F^o = n_F^i + 2x_{CH_4}^i n_F^i. \quad (8)$$

Similarly for the cathode, $n_A^o = \sum n_k^i - \frac{I}{4F}$, where $k = \{O_2, N_2\}$.

One can show that inlet/outlet mass flow rates at the anode and cathode streams can be related to $n_F^o, n_F^i, n_A^o, n_A^i$ as follows:

$$\begin{aligned} W_F^o &= M_{EQ,F}^o n_F^o \\ W_A^o &= M_{EQ,A}^o n_A^o \\ W_F^i &= M_{EQ,F}^i n_F^i \\ W_A^i &= M_{EQ,A}^i n_A^i \end{aligned} \quad (9)$$

where $M_{EQ,F}^{(\cdot)} = \sum M_{k,F} \cdot x_{k,F}^{(\cdot)}$, $k = \{H_2, \dots, CH_4\}$ and $M_{EQ,A}^{(\cdot)} = \sum M_{k,A} \cdot x_{k,A}^{(\cdot)}$, $k = \{O_2, N_2\}$. $M_{(\cdot),F/A}$ are the molar masses of species (\cdot) at the fuel and air channels, respectively.

The state equations are obtained by substituting (5)–(10) into (3) and (4)

$$mc_v \frac{dT_S}{dt} = f_1 + g_{11} n_F^i + g_{12} I \quad (10)$$

and

$$\frac{V c_v}{R} \frac{dp_S}{dt} = f_2 + g_{21} n_F^i + g_{22} I \quad (11)$$

where the detailed expressions of $f_{(\cdot)}$ and $g_{(\cdot)}$ are given in the Appendix.

State equations for the catalytic burner are constructed in the form

$$\begin{aligned} \frac{dm_{cb}}{dt} &= W_{cb}^i - W_{Turb}^o \\ m_{cb} C_p \frac{dT_{cb}}{dt} &= W_{cb}^i c_v (T_{cb}^i - T_{cb}) \\ &\quad - R(T_{cb}^i W_{cb}^i - T_{cb} W_{Turb}^o) + Q_{CB} \end{aligned} \quad (12)$$

where the CB inlet flow rate W_{cb}^i is the sum of the anode and cathode outlet flows, namely $W_{cb}^i = W_A^o + W_F^o$. \dot{m}_{Turb}^o is the flow through the turbine and is expressed as a function of m_{cb}, T_{cb} using the orifice equation described in [19]. The hydrogen residue from the SOFC stack is assumed to be completely combusted in the CB and the heat production Q_{CB}

because of the oxidation is defined as the enthalpy change, $n_{H_2}^i(h_{H_2} + 0.5h_{H_2O})$. Using (10), (13) and (13) can be rewritten by

$$\frac{dm_{cb}}{dt} = f_3 + g_{31} \cdot n_F^i + g_{32} \cdot I \quad (14)$$

and

$$m_{cb}C_v \frac{dT_{cb}}{dt} = f_4 + g_{41} \cdot n_F^i + g_{42} \cdot I. \quad (15)$$

The pressure in CB is obtained by the ideal gas law, assuming that the pressure variation inside the chamber is negligible.

A shaft model represents the GT rotating dynamics

$$\alpha NJ \frac{dN}{dt} = P_T \eta_m - P_C - P_{GEN} \quad (16)$$

where N is the turbine speed in rpm and η_m is the turbine mechanical efficiency that accounts for energy losses due to friction. The turbocharger inertia J is the sum of the rotor inertia, compressor inertia, and turbine wheel inertia. The factor $\alpha = (2\pi/60)^2$ is a result of converting the speed from radian per second to revolutions per minute.

Assuming that the specific heat coefficients of air do not change, the power P_c required to drive the compressor can be related to the mass flow rate W_A^i and the rotor speed from the first law of thermodynamics as

$$\begin{aligned} P_c &= W_A^i c_{p|c} T_{c1} \frac{1}{\eta_c} \left(\left(\frac{p_{c2}}{p_{c1}} \right)^{\frac{\gamma-1}{\gamma}} - 1 \right) \\ &= W_A^i c_{p|c} T_{c1} \frac{1}{\eta_c} \left(v_{c0}(W_A^i, N)^{\frac{\gamma-1}{\gamma}} - 1 \right) \\ &= v_c(W_A^i, N) \end{aligned} \quad (17)$$

where $v_{c0}(W_A^i, N)$ is the parametric model of a pressure ratio from the compressor map as a function of mass flow and rotational speed [27].

Similarly, the turbine power is given by

$$\begin{aligned} P_t &= W_{Turb}^o c_{p|t} T_{t1} \eta_t \left(1 - \left(\frac{p_{t2}}{p_{t1}} \right)^{\frac{\gamma-1}{\gamma}} \right) \\ &= W_{Turb}^o(m_{cb}, T_{cb}) c_{p|t} T_{t1} \eta_t \left(1 - \left(\frac{m_{cb} R T_{cb}}{V_{cb} p_{t1}} \right)^{\frac{\gamma-1}{\gamma}} \right) \\ &= v_t(m_{cb}, T_{cb}). \end{aligned} \quad (18)$$

By (17) and (18), (16) can be rewritten as follows:

$$\alpha NJ \frac{dN}{dt} = v_t(m_{cb}, T_{cb}) \eta_m - v_c(W_A^i, N) - P_{GEN}. \quad (19)$$

Considering (10), (11), (14), (15), and (19), the nonlinear dynamic system of SOFC/GT can be represented by a five-state model as follows:

$$\dot{X} = f(X) + g_1(X)u_1 + g_2(X)u_2 + g_3(X)u_3 \quad (20)$$

where

$$X = \begin{bmatrix} T_S \\ p_S \\ m_{cb} \\ T_{cb} \\ N \end{bmatrix}; \quad \underline{u} = \begin{bmatrix} n_F^i \\ I \\ P_{GEN} \end{bmatrix} \quad (21)$$

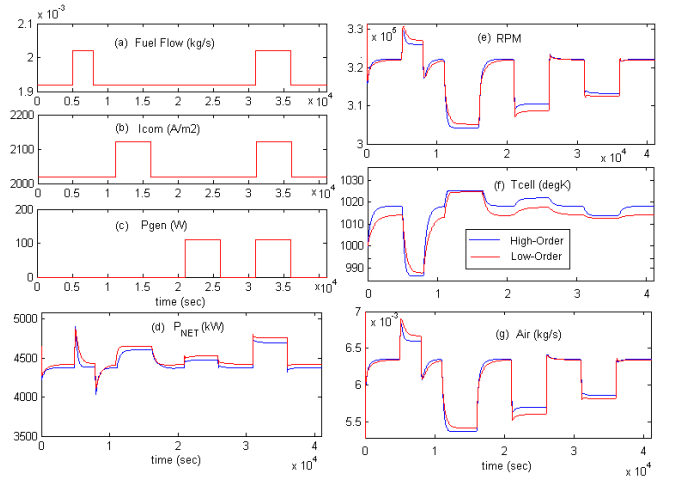


Fig. 6. Model validation results: inputs and performance variables. Blue = higher-order model. Red = lower-order model.

and $f(X) = D^{-1}\bar{f}(X)$, $g_1(X) = D^{-1}\bar{g}_1(X)/M_{EQ,F}^i$, $g_2(X) = D^{-1}\bar{g}_2(X)$, $g_3(X) = D^{-1}\bar{g}_3(X)$, $D = \text{diag}(m_{cb}c_v, \frac{V_{cb}}{R}, 1, m_{cb}c_v, \alpha NJ)$

$$\begin{aligned} \bar{f}(X) &= \begin{bmatrix} f_1 \\ f_2 \\ f_3 \\ f_4 \\ v_t(m_{cb}, T_{cb})\eta_m - v_c(\dot{m}_A^i, N) \end{bmatrix} \\ \bar{g}_1(X) &= \begin{bmatrix} g_{11} \\ g_{21} \\ g_{31} \\ g_{41} \\ 0 \end{bmatrix}; \bar{g}_2(X) = \begin{bmatrix} g_{12} \\ g_{22} \\ g_{32} \\ g_{42} \\ 0 \end{bmatrix}; \bar{g}_3(X) = \begin{bmatrix} 0 \\ 0 \\ 0 \\ 0 \\ -1 \end{bmatrix}. \end{aligned} \quad (22)$$

B. Model Validation

The validation of the model (20) is done by comparing its dynamic response with that of the 47-state model in [23] with step changes (up/down) of the three inputs, namely the stack current, the fuel flow, and the generator load, are applied at time 5000, 11 000, and 21 000 s to individual inputs, followed by the simultaneous step changes of all inputs at 31 000 s as shown in Fig. 6(a). The response of the key variables is shown in Fig. 6 together with that of the higher-order model. Note that the lower-order model response matches with the higher-order model, especially for the transient dynamics. The response shown in Fig. 6 also reveals dynamic characteristics of the SOFC/GT system that are important for consideration in the control design. With a step increase in fuel flow command (at 5000 s), the air to the stack increases because of the increase in power to the shaft, and it leads to a drop in the SOFC temperature. The fuel step change has very little influence on the net power except the transient phase. At 11 000 s where the step of stack current is applied, the power increases sharply in the initial phase and then followed by a gradual increase. This gradual power increase is a result of the increase in the stack temperature. The step of generator load command at 21 000 s reduces the cooling effect, thus leading to more heat being

TABLE II
SOFC OPERATING CONDITION FOR THE CASE STUDY

| | |
|---------------------------|---|
| Operating Pressure (bar) | 2.5 |
| Inlet gas temperature (K) | 750 |
| Inlet fuel composition | H_2 32.58%, H_2O 3.85%, CO 16.29%, CO_2 1.92%, CH_4 0.24%, N_2 45.12%, |
| Inlet air composition | O_2 21%, N_2 79% |

generated from stack. It can be seen that, despite some offset, the reduced-order model captures the essential dynamic I/O behavior of the higher-order model.

IV. MODEL PREDICTIVE CONTROL FOR THE SOFC/GT COMBINED CYCLE SYSTEM

With the five-state MIMO nonlinear model of (20), we proceed to develop the MPC by formulating the following optimization problem:

$$\min_{\underline{u}_k, \dots, \underline{u}_{k+N_p}} \left[\begin{aligned} J_k &= \sum_{n=1}^{N_p} (P_{NET,k+n} - P_{SET,k+n})^2 \\ &+ (\underline{u}_{k+n} - \underline{u}_{SET,k+n})^T \Gamma (\underline{u}_{k+n} - \underline{u}_{SET,k+n}) \end{aligned} \right] \quad (24)$$

[.2pt] subject to

$$\begin{aligned} X_{k+1} &= f(X_k) + g(X_k)\underline{u}_k \quad (25) \\ T_{CELL}^{\min} &\leq T_{CELL,k+n} \leq T_{CELL}^{\max} \\ W_{Fuel}^{\min} &\leq W_{Fuel,k+n} \leq W_{Fuel}^{\max} \\ I_{com}^{\min} &\leq I_{COM,k+n} \leq I_{com}^{\max} \\ P_{GEN}^{\min} &\leq P_{GEN,k+n} \leq P_{GEN}^{\max} \\ \Delta I_{com}^{\min} &\leq I_{COM,k+n} - I_{COM,k+n-1} \leq \Delta I_{com}^{\max} \quad (26) \end{aligned}$$

where $n = 0, \dots, N_p$ and (25) is a discrete-time representation of the nonlinear hybrid model given by (20). N_p is the prediction horizon. $P_{NET,k}$ and $P_{SET,k}$ are the net power and demanded power at time instant, k , respectively. $\underline{u}_k = [W_{Fuel,k}, I_{COM,k}, P_{GEN,k}]^T$ and $\Gamma = \text{diag}(r_1, r_2, r_3)$ is the control weighting matrix which can be used as tuning parameter for the MPC design. The variables with subscript SET denote the reference trajectories. The upper and lower limits of the state and input constraints are defined based on the steady-state load operation maps. An acceptable rate change is placed on the current as rapid variation on current will harm the fuel cell. The optimization problem (24)–(26) is solved for each time step k using *fmincon* in MATLAB.

The MPC design and tuning are illustrated using a case study. Consider the step change from 5900 to 5300 W. Even though this seems to be a moderate step power change, the specified step load profile clearly demonstrates the non-monotonic temperature property. Moreover, the corresponding optimal steady-state operating condition is very close to the SOFC temperature boundary. We use a sampling frequency of 2 Hz and the current rate of change is limited by $|I_{CELL,k+1} - I_{CELL,k}| \leq 30 \text{ A/m}^2$. The cell temperature is constrained by $T_{CELL} \leq 983 \text{ K}$. The operating conditions for the SOFC are specified in Table II. The control horizon is chosen equal to the prediction horizon. The prediction horizon (N_p) is tuned while different weightings (r_1, r_2, r_3) are applied to

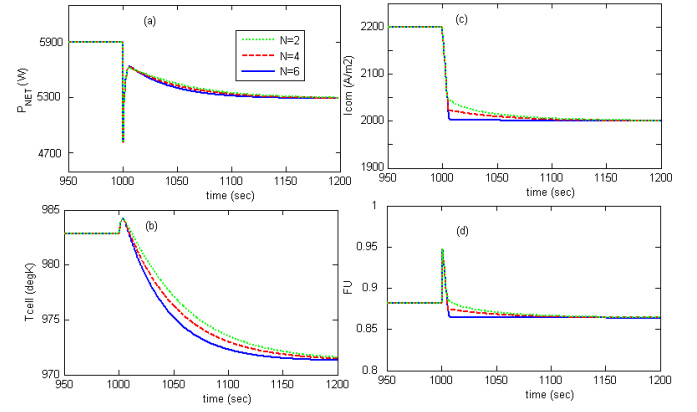


Fig. 7. Closed-loop responses of the current-based MPC for different prediction horizon values: (a) net power, (b) SOFC temperature, (c) current, and (d) fuel utilization. When the power demand jumps from 5900 to 5300 W, the cell temperature exceeds the temperature limit, or $T_{CELL}^{\max} = 983 \text{ K}$.

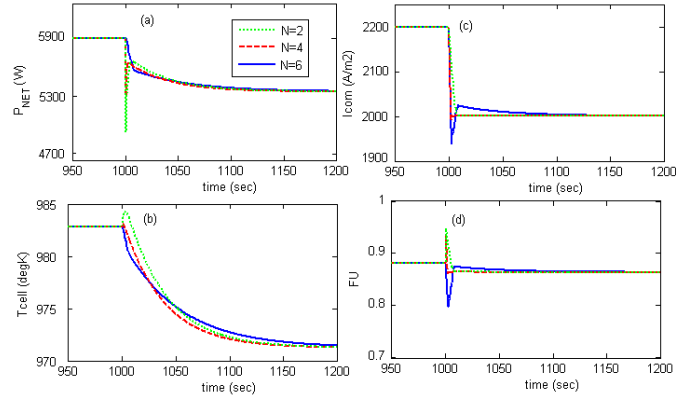


Fig. 8. Closed-loop responses of the MPC with current and fuel as active controls: (a) net power, (b) SOFC temperature, (c) current, and (d) fuel utilization.

compare the MPC performance under three different control coordinations. More specifically: 1) the fuel and generator load are set to the optimal set points while the current is manipulated (current-based MPC); 2) the current and fuel are concurrently manipulated (fuel/current combined MPC) and the generator load is fixed at the optimal set point; and 3) all three control elements are changed freely.

The input and output signals obtained using the current-based MPC algorithm are shown in Fig. 7. The high penalty values ($r_1 = 200, r_3 = 200$) are used to suppress the fuel and generator load actuation. It can be seen that the proposed MPC strategy tracks the power demand closely with no steady-state offset. However, substantial power tracking error occurs when the system is running into near-fuel starvation condition as FU reaches a very high value of 95% as shown in Fig. 7. Even with the increased prediction horizon, the proposed current-based MPC controller could not prevent constraint violation because of current rate limit during the power step-down transient. Moreover, this constraint is active for the longest time period when $N_p = 6$ in Fig. 3.

Because managing a cell temperature within the prespecified limit is not achievable, given the weak control authority of the

current-based MPC scheme, additional control design degree-of-freedom, namely a fuel flow, is used to meet the fuel cell thermal constraints. As shown in Fig. 8(b), temperature constraint is enforced with the fuel as an additional control. Under the low FU condition, the stack temperature decreases because of the increased cooling effect. More fuel is supplied to the fuel cell during transient. This in turn results in feeding more cold air to the cathode side which carries away the heat from the fuel cell stack. In contrary to the current-based MPC, simulation shows that the closed-loop response to the combined current and fuel MPC is substantially influenced by the prediction horizon N_p . The temperature margin tends to increase with an increase in the prediction horizon. The transient power tracking performance is also enhanced by adding fuel as the control, which can be rapidly activated to avoid the high FU condition and thereby reducing the excessive power deviation.

The weighting matrix γ is also used as the main tuning parameters to shape the closed-loop response for desired performance. The numerical values of the different gains used for simulations are $r_2 = 100, 10$. In our simulation, the value of r_2 in the range of [8, 100] yields reasonable load following performance. However, it is observed that the cell temperature is insensitive to the penalty parameter variation, as shown in Fig. 9.

The power transient performance is further improved by implementing a generator load control which can rapidly respond to contribute to the total system power. Fig. 9 compares the control performance in terms of the power and thermal responses when the generator load is used as a control variable. The transient power excursion is reduced by 40% and fast load following is achieved, thanks to the generator load. Further performance improvement can be achieved by the turbine design with a large power split ratio or by operating the electrical machine as both the generator and the motor [29].

The MPC for the SOFC/GT load following the control proposed here has moderate computational complexity and is feasible for implementation on standard hardware. For example, the optimization problem with 0.5 s sampling interval and six-step predictive horizon can be solved in 0.18 s in simulations on a desktop computer with 2.4 GHz CPU and 2 GB RAM. This moderate computational demand makes the MPC power and thermal control promising for real-time implementation. It should be noted that while MPC provides a flexible and advanced control design framework for constrained dynamic systems, it also raises several issues whose complete solutions are yet to be developed. One of these issues is that successive feasibility of the optimization problem is in general not guaranteed, as it is the case for the problem being investigated in this paper. One mitigate solution to avoid the numerical issues associated with the loss of feasibility is to reformulate the optimization problem, namely, to convert the hard constraints into soft constraints. The reformulated soft-constrained optimization problem will not have feasibility issues, yet it does not guarantee that the original hard constraints can always be enforced.

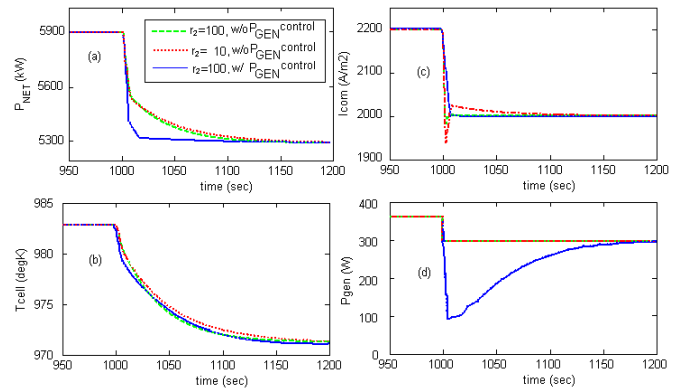


Fig. 9. Closed loop response of the MPC with different weightings and with current, fuel, and generator load as controls: (a) net power, (b) SOFC temperature, (c) current, and (d) generator power.

Although this paper presents the investigation of the SOFC/GT for a small scale, similar models can be derived following the same modeling approach for larger systems. In general, they will require more discrete cells to capture the temperature gradient and pressure distribution. The power split between SOFC and GT will also depend on the rated power of the overall system. Component sizing of SOFC/GT systems, which refers to the proper selection of individual component physical parameters, is an important step in system integration. The sizing of the system is, however, not addressed in this paper, and will be pursued in our future publications.

V. CONCLUSION

This paper presents an MPC scheme for power-tracking and thermal management, and illustrates its effectiveness in dealing with various constraints. Although most constraints are because of physical limits or operational safety considerations of components, the inclusion of the rate limit on the SOFC current is primarily out of the concern that the slow response of fuel reformer system could lead to fuel starvation if the current changes very fast. The flexible formulation of the MPC cost function allows us to evaluate the sensitivity of the control performance to different control input combinations and other MPC design parameters. By choosing different weighting matrices, we designed the current-based (by highly penalizing the fuel and generator load change), coordinated current and fuel (highly penalizing P_{GEN}), and the MIMO (with all inputs used) MPCs and evaluated and compared their performances.

Our case study leads to the conclusion that, with the help of the reduced-order model, the MPC is feasible for simultaneous power tracking and thermal management, and can deal with both input and state constraints effectively. Moreover, the flexible MPC formulation and its capability in dealing with MIMO problem make the controller tuning easier and more intuitive than other MIMO design methodologies. The MPC with moderate weight and long prediction horizon on the fuel and current is proved to be effective in achieving both temperature and power regulation of the SOFC/GT hybrid system. The generator load was utilized as an effective mechanism to mitigate the power deviation during load transition.

APPENDIX

Detailed Expressions of $f_{(\cdot)}$ and $g_{(\cdot)}$ in Section III-A.

$$\begin{aligned}
f_1 &= M_{EQ,A}^i n_A^i (c_v T_i - c_v T_S - RT_i) - RT_S M_{EQ,A}^o n_A^i \\
g_{11} &= -RT_i M_{EQ,F}^i + c_v (T_i - T_S) M_{EQ,F}^i + M_{EQ,F}^o (1 + 2x_{CH_4}^i) \\
g_{12} &= \frac{1}{2F} (h_{H_2} + 0.5h_{O_2} - h_{H_2O}) - \dot{U} + RT_S M_{EQ,A}^o \cdot \frac{1}{4F} \\
f_2 &= f_1 + c_v M_{EQ,A}^i n_A^i - M_{EQ,A}^o n_A^i \\
g_{21} &= g_{11} + c_v M_{EQ,F}^i + M_{EQ,F}^o (1 + 2x_{CH_4}^i) \\
g_{22} &= g_{12} + c_v M_{EQ,F}^o \frac{1}{4F} \\
f_3 &= M_{EQ,A}^o n_A^i + M_{EQ,F}^o 2x_{CH_4}^i - W_{Turb}^o \\
g_{31} &= M_{EQ,F}^o \\
g_{32} &= -M_{EQ,A}^o \cdot \frac{1}{4F} \\
f_4 &= (M_{EQ,A}^o n_A^i + M_{EQ,F}^o 2x_{CH_4}^i) c_v (T_i - T_{CB}) - RT_i M_{EQ,A}^o n_A^i - RT_i M_{EQ,F}^o 2x_{CH_4}^i \\
&\quad + RT_{CB} (M_{EQ,A}^o n_A^i + M_{EQ,F}^o 2x_{CH_4}^i - \dot{m}_{Turb}^o) - \Delta n_{CO} (h_{H_2} + 0.5h_{O_2} - h_{H_2O}) \\
g_{41} &= M_{EQ,F}^o c_v (T_i - T_{CB}) - RT_i M_{EQ,F}^o + RT_{CB} M_{EQ,F}^o + (h_{H_2} + 0.5h_{O_2} - h_{H_2O}) 3x_{CH_4}^i \\
g_{42} &= -M_{EQ,A}^o \cdot \frac{1}{4F} c_v (T_i - T_{CB}) + RT_i M_{EQ,A}^o \cdot \frac{1}{4F} - RT_{CB} M_{EQ,A}^o \cdot \frac{1}{4F} - (h_{H_2} + 0.5h_{O_2} - h_{H_2O}) \cdot \frac{1}{2F}
\end{aligned}$$

REFERENCES

- [1] S. C. Singhal and K. Kendall, *High Temperature Solid Oxide Fuel Cells*. New York, NY, USA: Elsevier, 2003.
- [2] S. Campanari, "Power plants based on solid oxide fuel cells combined with gas turbine cycles," Ph.D. dissertation, Dept. Energy Sci., Politecnico di Milano Univ., Milan, Italy, 1998.
- [3] J. Larminie and A. Dicks, *Fuel Cell System Explained*. New York, NY, USA: Wiley, 2004.
- [4] A. Palsson, A. Selimovic, and L. Sjunnesson, "Combined solid oxide fuel cell and gas turbine systems for efficient power and heat generation," *J. Power Sour.*, vol. 86, nos. 1–2, pp. 442–448, 2000.
- [5] *Fuel Cell Handbook*, 7th ed., U.S. Department of Energy, National Energy Technology Laboratory, Morgantown, WV, USA, 2004.
- [6] R. Kandepu, B. A. Foss, and L. Imsland, "Integrated modeling and control of a load-connected SOFC-GT autonomous power system," in *Proc. Amer. Control Conf.*, Minneapolis, MN, USA, Jun. 2006.
- [7] J. E. Freeh, C. J. Steffen, and L. M. Larosiliere, "Off-design performance analysis of a solid-oxide fuel cell/gas turbine hybrid for auxiliary aerospace power," in *Proc. 3rd Int. Conf. Fuel Cell Sci. Eng. Technol.*, 2005, pp. 265–272.
- [8] A. Himansu, J. E. Freeh, C. J. Steffen, R. T. Tornabene, and X. J. Wang, "Hybrid solid oxide fuel cell/gas turbine system for high altitude long endurance aerospace missions," in *Proc. 4th Int. Conf. Fuel Cell Sci. Eng. Technol.*, 2006, pp. 573–583.
- [9] R. Fang, W. Jiang, J. Khan, and D. Roger, "System-level thermal modeling and co-simulation with hybrid power system for future all electric ship," in *Proc. IEEE Electr. Ship Technol. Symp.*, Apr. 2009, pp. 547–553.
- [10] J. Sun, J. Stebe, and C. Kennell, "Feasibility and design implications of fuel cell power for sealift ships," *Naval Eng. J.*, vol. 22, no. 3, pp. 87–102, 2010.
- [11] M. J. Brear and M. J. Dunkley, "The effect of size on optimization of solid oxide fuel cell/gas turbine hybrid cycles," *ASME J. Eng. Gas Turbines Power*, vol. 132, no. 9, pp. 094502-1–094502-4, 2010.
- [12] N.-S. Myung, S.-K. Park, and T.-S. Kim, "Analysis of performance of SOFC/GT hybrid systems considering size-dependent performance of gas turbines," *Trans. Korean Soc. Mech. Eng.*, vol. 35, no. 4, pp. 399–407, 2011.
- [13] D. Stephenson and L. Ritchey, "Parametric study of fuel cell and gas turbine combined cycle performance," ASME, New York, NY, USA, Tech. Rep. 97-GT-340, 1997.
- [14] C. Stiller, B. Thorud, and O. Bolland, "Safe dynamic operation of a simple SOFC/GT hybrid system," in *Proc. GT2005, ASME Turbo Expo, Power Land, Sea and Air*, NV, USA, 2005.
- [15] F. Mueller, F. Jabbari, J. Brouwer, R. Roberts, T. Junker, and H. Ghezal-Ayagh, "Control design for a bottoming solid oxide fuel cell gas turbine hybrid system," *J. Fuel Cell Sci. Technol.*, vol. 4, no. 3, pp. 221–230, 2007.
- [16] C. Wechter, R. Lunderstdt, and F. Joos, "Dynamic model of a pressurized SOFC/gas turbine hybrid power plant for the development of control concepts," *J. Fuel Cell Sci. Technol.*, vol. 3, no. 3, pp. 271–279, 2006.
- [17] H. Xi, "Dynamic modeling and control of planar SOFC power systems," Ph.D. dissertation, Univ. Michigan, Ann Arbor, MI, USA, 2007.
- [18] D. J. Hall, "Transient modeling and simulation of a solid oxide fuel cell," Ph.D. Dissertation, Univ. Pittsburgh, Pittsburgh, PA, USA, 1997.
- [19] V. Tsourapas, "Control analysis of integrated fuel cell systems with energy recuperation devices," Ph.D. dissertation, Univ. Michigan, Ann Arbor, MI, USA, 2007.
- [20] C. Stiller, B. Thorud, S. Seljebo, O. Mathisen, H. Karoliussen, and O. Bolland, "Finite-volume modeling and hybrid-cycle performance of planar and tubular solid oxide fuel cells," *J. Power Sour.*, vol. 141, no. 2, pp. 227–240, 2005.
- [21] R. A. Roberts and J. Brouwer, "Dynamic simulation of a pressurized 220 kW solid oxide fuel-cell gas-turbine hybrid system: Modeled performance compared to measured results," *J. Power Sour.*, vol. 3, no. 1, pp. 18–25, 2006.
- [22] R. A. Roberts, J. Brouwer, F. Jabbari, T. Junker, and H. Ghezal-Ayagh, "Control design of an atmospheric solid oxide fuel cell/gas turbine hybrid system: Variable versus fixed speed gas turbine operation," *J. Power Sour.*, vol. 161, no. 1, pp. 484–491, 2006.
- [23] S.-R. Oh and J. Sun, "Optimization and load-following characteristics of 5 kw-class tubular solid oxide fuel cell/gas turbine hybrid systems," in *Proc. Amer. Control Conf.*, Baltimore, MD, USA, 2010, pp. 417–422.
- [24] S.-R. Oh, J. Sun, H. Dobbs, and J. King, "Comparative performance assessment of 5 kW-class solid oxide fuel cell engines integrated with single/dual-spool turbochargers," in *Proc. Amer. Control Conf.*, San Francisco, CA, USA, 2011, pp. 5231–5236.
- [25] S.-R. Oh, J. Sun, H. Dobbs, and J. King, "Model-based predictive control strategy for a solid oxide fuel cell system integrated with a turbocharger," in *Proc. Amer. Control Conf.*, Montreal, QC, Canada, 2012.
- [26] P. Aguiar, C. S. Adjiman, and N. P. Brandon, "Anode-supported intermediate temperature direct internal reforming solid oxide fuel cell. I: Model-based steady-state performance," *J. Power Sour.*, vol. 138, nos. 1–2, pp. 120–136, 2004.
- [27] J. Pukrushpan, A. Stefanopoulou, and H. Peng, *Control of Fuel Cell Power Systems: Principles, Modeling, Analysis, and Feedback Design*. London, U.K.: Springer-Verlag, 2004.
- [28] L. Eriksson, J. Wahlström, and M. Klein, "Physical modeling of turbocharged engines and parameter identification," in *Automotive Model Predictive Control* (Lecture Notes in Control and Information Sciences), vol. 402. New York, NY, USA: Springer-Verlag, 2010, pp. 53–71.
- [29] Z. Jia, J. Sun, S. Oh, H. Dobbs, and J. King, "Control of the dual mode operation of generator/motor in SOFC-GT-based APU for extended dynamic capabilities," *J. Power Sour.*, vol. 235, pp. 172–180, Aug. 2013.



So-Ryeok Oh received the B.S. and M.S. degrees from Pusan National University, Pusan, Korea, in 1997 and 1999, respectively, and the Ph.D. degree from the University of Delaware, Newark, DE, USA, in 2006.

He carried out research studies of ship maneuvering as a Research Associate from 2008 to 2012, he worked on a fuel cell/gas turbine hybrid system as an Assistant Research Scientist with the Naval Architecture and Marine Engineering Department, University of Michigan, Ann Arbor, MI, USA. His current research interests include modeling, design, and control of multibody robotic, and hybrid energy systems.



Jing Sun (F'04) received the B.S. and M.S. degrees from the University of Science and Technology of China, Hefei, China, in 1982 and 1984, respectively, and the Ph.D. degree from the University of Southern California, Los Angeles, CA, USA, in 1989.

She was an Assistant Professor with the Electrical and Computer Engineering Department, Wayne State University, Detroit, MI, USA, from 1989 to 1993. She joined Ford Research Laboratory, in 1993, where she was with the Powertrain Control Systems Department. She joined the faculty of the College of

Engineering, University of Michigan Ann Arbor, MI, USA, in 2003, where she is currently a Professor with the Department of Naval Architecture and Marine Engineering and the Department of Electrical Engineering and Computer Science. She holds 37 U.S. patents and has co-authored *Robust Adaptive Control* (Dover Publications, 2012). Her current research interests include system and control theory and its applications to marine and automotive propulsion systems.

Dr. Sun is one of the three recipients of the 2003 IEEE Control System Technology Award.



Joel King graduated from the Rensselaer Polytechnic Institute, Troy, NY, USA, and received the master's degree from the Naval Postgraduate Institute.

He is a Division Manager and an Assistant Vice President of Alion Science and Technology, and has provided engineering services support in the areas of fuel cells and non-primary power systems to the U.S. Army's Tank-Automotive Research Development and Engineering Center since 2003. He oversaw the operation, maintenance, and repair of conventional and nuclear powered propulsion plants.

He served in other operational sea duty assignments. He was the Officer in Charge of the Atlantic Fleet Force Nuclear Propulsion Mobile Training Team. He holds Nuclear Engineer Officer's Certification from the Naval Nuclear Propulsion Program.



Herbert Dobbs received the Bachelor of Science degree in chemical engineering from Iowa State University, Ames, IA, USA, and the master's degree in mechanical engineering from the University of Michigan-Dearborn, Dearborn, MI, USA.

He is a Licensed Professional Engineer. He was with the U.S. Army RDECOM-TARDEC in vehicle power and propulsion related areas, including fuel cells and JP-8 fuel reforming, propulsion system cooling, air cleaners, gas turbine engine technology, auxiliary power systems, integrated diesel engine

and fuel cell power systems, hybrid electric propulsion, and synthetic fuel qualification. He works for the Non-primary Power Systems Team, TARDEC's Ground Vehicle Power and Mobility Area, where he leads projects to develop fuel cell and fuel reforming technologies for use in robot and vehicle auxiliary power. He has worked in nuclear biological and chemical protection for vehicles, and as TARDEC's technology transfer officer.